Korean J. Chem. Eng., 39(9), 2307-2317 (2022)
DOI: 10.1007/s11814-022-1142-z

pISSN: 0256-1115
eISSN: 1975-7220

Optimal strategies for supercritical gas antisolvent (GAS) coprecipitation of pyrazinamide/PVP particles via response surface methodology

Azadeh Shirafkan*, Seyed Mostafa Nowee*,†, and Hossein Kamali,*****

*Chemical Engineering Department, Faculty of Engineering, Ferdowsi University of Mashhad, Mashhad, Iran
**Department of Pharmaceutics, Faculty of Pharmacy, Mashhad University of Medical Sciences, Mashhad, Iran
***Targeted Drug Delivery Research Center, Pharmaceutical Technology Institute,
Mashhad University of Medical Sciences, Mashhad, Iran
(*Received 1 March 2022 • Revised 6 April 2022 • Accepted 10 April 2022*)

Abstract−This paper concerns optimization and experimental validation of coprecipitation process parameters for preparing particles of Pyrazinamide and Polyvinylpyrrolidone using gas anti-solvent supercritical method. Mixtures of organic solvents (acetone and ethanol) were selected with various combinations of the drug and the polymer. The central composite design (CCD) was adopted to explore the effect of temperature, pressure, antisolvent addition rate, polymer fraction, and ethanol fraction on particle size distribution (PSD) and solubility. The strong likelihood models were developed for all the responses using Design-Expert software. Polymer fraction was the most important ($p<0.0001$) factor influencing PSD, while pressure and interaction between temperature and polymer fraction significantly affected solubility. The optimal condition was specified at temperature of 50 °C, pressure of 120 bar, antisolvent rate of 16 bar/min, polymer fraction of 30%, and ethanol fraction of 50%. The model was then validated experimentally under the optimal condition and compared with pure PZA and particles obtained from the physical mixture. According to DLS, XRD, FTIR, and FESEM analyses, the crystallinity of PZA-PVP particles was reduced in optimum conditions, leading to higher solubility. Also, the results suggest that it is feasible to produce coprecipitated particles with narrower size distribution by optimized GAS process.

Keywords: Central Composite Design, Gas Antisolvent Supercritical, Polyvinylpyrrolidone, Pyrazinamide, Response Surface Methodology

INTRODUCTION

Pyrazinamide (pyrazine-2-carboxamide; PZA), as an essential antitubercular agent, is a white powder with the molecular formula of $C_5H_5N_3O$. This medicinal combination has been proposed by the World Health Organization for treating patients with tuberculosis. Since the pyrazinamide-free treatment regimen lasts for nine months or more, this substance can provide an easier treatment for patients in a shorter period of time (six months) [1,2]. However, hepatotoxicity, which depends on the drug dose, is considered the most severe side effect of this medicine [3]. Now, to deal with this problem, it is recommended to use hydrophilic polymeric carriers, the efficacy of which has been proven in improving chronic diseases such as tuberculosis. These compounds can pass the biological barriers and target mycobacterium tuberculosis cellular reservoirs [3-5]. In fact, the amorphous structure of medicines by polymers has affected the solubility of the active compound in the hydrophilic environment of the human body, delivered the drug to the desired location, reduced the drug dose, and ultimately improved the efficacy [6]. According to the studies, poly vinyl-pyrrolidone (PVP) can be considered as a hydrophilic polymer among other polymers as a proper stabilizing agent to prevent crystallization and particle growth. Additionally, reducing the particle size followed by increasing the surface-to-volume ratio of the active pharmaceutical ingredients (APIs) is known as effective for increasing the drug solubility [5]. Currently, conventional methods such as solvent evaporation, spray drying, and jet milling are used to micronize APIs; but there are problems associated with these methods, which include lack of proper control over particle morphology, practical difficulties in solvent removal, high-pressure operations [7], particle degradation due to thermal and mechanical stress, and finally the time-consuming process of particle production [8]. Over the years, attention has been drawn to supercritical fluid (SCF) as a green and clean technology in many fields, especially in producing sensitive and valuable drug compounds. The unique features of SCFs in the industrial use, pharmaceutical industry in particular, include modifying the particle size distribution (PSD) and SCF solubility with a slight change in temperature and system pressure, applying mild critical conditions, especially in terms of temperature (T_c in the temperature range of 25-40 °C) for temperature-sensitive compounds, and producing a high-quality product without residual solvents. Moreover, supercritical carbon dioxide ($scCO_2$) is a common solvent due to some features such as non-toxicity, low price, low viscosity, mild critical conditions, and availability [9-11]. Among process precipitation methods, gas anti-solvent supercritical (GAS) method is regarded as the most efficient and preferred method for micronizing or nanosizing particles, since many organic compounds, as well as polymers, are insoluble and poorly soluble in supercritical fluid [12-14]. In such

†To whom correspondence should be addressed.
E-mail: nowee@ferdowsi.um.ac.ir

circumstances, SCFs play an anti-solvent role for the solute; as a result, $scCO_2$ solubility is considered a sensitive and determining factor in choosing the supercritical process [15]. In the GAS process, the solubility of the organic solvent in the SCF causes considerable volume expansion followed by decreased solvent strength. Eventually, nucleation and crystal growth occur due to high supersaturation, which will lead to particle precipitation. The last step in the process is to remove the remaining solvent with the excess flow of $scCO_2$ and the dry particles can be collected after evacuation and pressure drop [16-18]. The researchers found that using the mixture of organic solvent and changes in their content composition produced high-efficiency nanoparticles [17,19]. Using polymeric carriers, PVP in particular, has been the focus of other studies that affect morphology, size distribution, and solubility of APIs [20-23]. Hence, it can be inferred that using polymer components would improve the medicinal properties. Numerous studies have been conducted on producing micro-and nano-particles of various compounds, especially pharmaceutical compounds, by the GAS process to increase the solubility of these substances in aqueous media [24-27]. However, a small number of works in recent years have focused on model-based optimization of the GAS process, where in addition to operating parameters (such as temperature, pressure, and antisolvent addition rate (AAR)), factors such as using organic solvent mixture as well as polymer carrier, alongside the drug composition, are considered. In the above-mentioned studies, the impact of various parameters on the process is addressed empirically.

In the present study, an optimizing GAS process based on the response surface methodology (RSM) approach is presented to produce PZA-PVP submicron particles using organic solvent combination of acetone and ethanol. The RSM-based model is used to estimate the optimal conditions for the operating parameters in order to achieve maximum solubility and produce smaller particles. Results of this optimization are implemented in the experimental study of this system that has been presented elsewhere in detail [28]. Finally, more experimental runs were conducted to validate the model, and the particles produced under the optimal conditions were analyzed and compared with the pure PZA and physical mixture of PZA-PVP, respectively.

MATERIALS AND METHODS

1. Materials

Pyrazinamide (99% purity) was purchased from Tinab Shimi Chemical Company (Iran) and PVP-k30 (~30,000-50,000 g/mol) was obtained from Sigma-Aldrich (Germany). CO_2 (99% purity) was acquired from Toos Co (Iran). Ethanol and acetone (analytical grade) were obtained from the Merck company (Germany), and deionized water was used for solubility studies.

2. Preparation of PZA-PVP Particles by GAS Process

In previous work, the GAS process was successfully applied to obtain experimental results for coprecipitation of PZA-PVP particles under various conditions [28]. In this study, the same experimental method was employed to modify the operating parameters and then validate experimentally the model for the purpose of a satisfactory outcome. Thereby, the minimum mean particle size and maximum solubility was implemented using the GAS system. Fig. 1 shows the schematic flow diagram of the apparatus, jacketed precipitation chamber and control system. In all experiments, solutions of PZA and PVP, at polymer/drug mass ratio of 0/1, 1/10, 1/5, 1/2, and 2/3, in a 50 ml ethanol-acetone mixture (with the specific volume fraction) were provided. Then the prepared solution was loaded into the precipitation chamber (internal volume of 700 cm^3), which had a temperature-controlled jacket equipped with a circulating water bath (model WCR-P8, Wise Circu, Korea) to heat it to the operation temperature. When the system temperature became stable at the desired setpoint, the precipitation chamber was pressur-

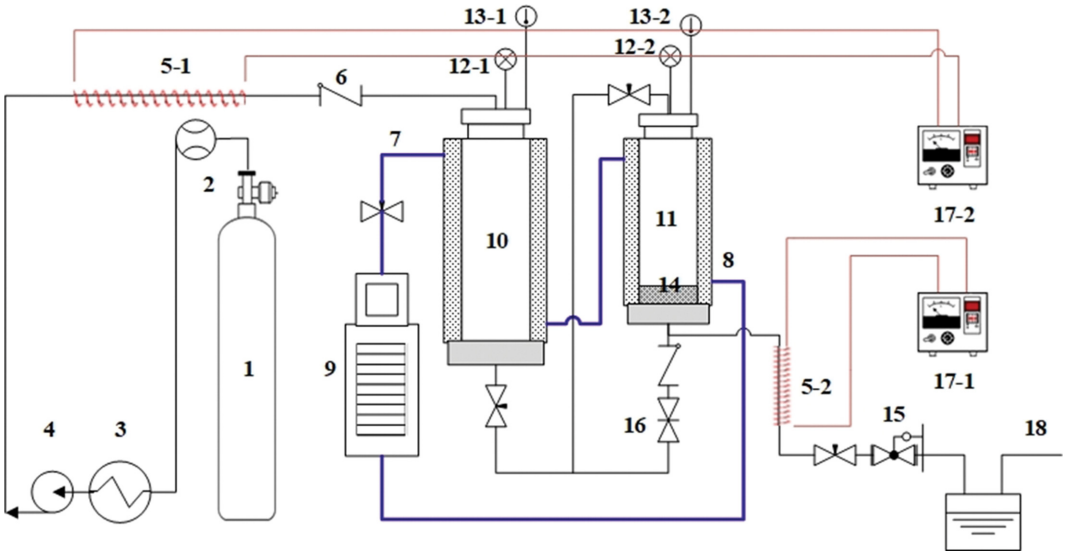

Fig. 1. Experimental setup of the GAS process: (1) CO_2 cylinder, (2) flowmeter, (3) heat exchanger, (4) high-pressure pump, (5-1, 5-2) band heater, (6) check valve, (7) inlet stream of heated jacket, (8) outlet stream of heated jacket, (9) circulator, (10) pulse dampener, (11) precipitator, (12-1, 12-2) pressure transmitter, (13-1, 13-2) temperature transmitter, (14) sintered metal filter and membrane (15) back-pressure regulator, (16) micro needle valve, (17-1, 17-2) power supply, (18) vent.

ized up to the target point with CO_2 flow rate using a high-pressure pump (model M72, MAXIMATOR, Germany) through a stainless-steel tubing at the bottom of the chamber. Initially, CO_2 was flowed through a heat exchanger to be cooled by ethylene glycol to prevent any cavitation within the pump. Then a pulse dampener vessel (internal volume of 980 cm^3) was in place to reduce stream fluctuations generated by the pump before entering the precipitation chamber. CO_2 flow rate (antisolvent addition rate) was controlled manually using a micro needle valve. Once the desired amount of supercritical stream entered the precipitation chamber, the input stream was closed and the vessel was kept steady for at least 60 min. The $scCO_2$ contacted the organic solution, which led to a volumetric expansion and a decrease in the solvation power of the organic solvent; thus particle precipitation was fulfilled. Then, to eliminate excess organic solvent, $scCO_2$ was continuously pumped into the precipitation chamber from the top and discharged from the bottom line. $ScCO_2$ flowed for at least two hours at a constant rate by the manually controlled back pressure regulator (TESCOM, USA). After depressurization, the precipitated powder was collected for further analysis.

3. Preparation of PZA-PVP Particles by Physical Mixture

A physical mixture of PZA and PVP was prepared at the optimized polymer/drug mass ratio. To this end, the sieved fraction of both samples (PZA and PVP, <250 μm) was gently mixed using a spatula for 2 min prior to analysis.

4. Characterization of Precipitates

A particle size analyzer (Cordouan, Mod. Vasco3, France), based on dynamic light scattering (DLS), was employed to analyze mean volume diameter and particle size distribution. A summary of the results is presented in Table 2.

The X-Ray diffraction (XRD) patterns were acquired by a GNR X-Ray Explorer, which defined the crystallinity of the coprecipitated powders. The samples were exposed to radiation using a Cu anode (Cu-Kα=1.54 Å) at an output voltage of 40 kv and output current of 30 mA; the scanning angular range was recorded in 2θ interval from 5-60°.

FT-IR spectra were obtained using a Thermo Nicolet Avatar 370 spectrometer (USA) with a resolution of 4.0 cm^{-1}. The preparation of powder samples with reference material (KBr) in the form of pellets was needed for radiation. The absorption spectrum in the 4,000-400 cm^{-1} wavenumber range was recorded for each sample.

The morphology of processed particles was examined by field emission scanning electron microscope (FESEM, TESCAN $MIRA_3$, Czech Republic) at 10 kV accelerating voltage. For FESEM sample preparation, the powdered sample was coated with a thin gold layer to inhibit sample charging.

Analysis of saturation solubility of pure PZA and GAS processed samples was in accord with the previous works [29]. An excess amount of PZA was dispersed in deionized water (20 ml). The suspensions were placed in a shaker incubator at 100 rpm at 25 °C for 48 h. The samples were filtered through a 0.2 μm filter and analyzed using a double beam UV/VIS spectrophotometer (Rayleigh, Mod. UV-2601) at a wavenumber of 269 nm.

5. Experimental Design and Statistical Analysis

As mentioned, in the GAS process, the shape and size of particles affecting solubility depend on parameters such as temperature, pressure, antisolvent addition rate, mass fraction of the polymer in PZA-PVP mixture, and organic solvent ratios. Thus, to explore the optimal process variables, RSM based on a central composite design (RSM-CCD) was used to analyze the effect of these independent variables on the particle size distribution and solubility as system responses. CCD is a second-order design which is applied to analyze experimental error and includes all the combinations of two variables and central condition in three dimensions. In this study, the independent variables such as temperature (a), pressure (b), antisolvent addition rate (c), polymer fraction in PZA-PVP mixture (d), and ethanol fraction in the solvent mixture (e) are selected as basic parameters in the GAS precipitation system. Each variable is modified at five levels and the values of each are presented in Table 1.

Process behavior is described by a second-order polynomial equation as follows:

$$Y = b_0' + \Sigma_{i=1}^{n} b_i x_i + \Sigma_{i=1}^{n} b_{ii} x_i^2 + \Sigma_{i=1}^{n} . \Sigma_{j\geq 1}^{n} b_{ij} x_i x_j \quad (1)$$

where Y is the predicted system response, b_0', b_i, b_{ij}, and b_{ii} belong to fixed, linear, interaction, and quadratic coefficients, respectively. Also, x_i and x_j represent the uncoded independent variables [30,31].

RESULTS AND DISCUSSION

1. Optimization of Particle Size Distribution and Dissolution Rate Using RSM

In this study, five independent parameters were implemented at five levels by RSM-CCD to determine the system response, which were particle size and solubility. The range of the variables was selected based on primary tests and what is reported in literature. The experimental response, as well as the predicted response from 32 experimental tests at various levels of the independent variables and their interactions, are presented in Table 2. In practice, the particle precipitation did not occur for nine tests (runs 4, 5, 11, 12, 13, 17, 21, 24, and 28 in Table 2). In particular, experiments with

Table 1. Experimental range and levels in the GAS process

Variables	Symbols	Range and level				
		−2	−1	0	1	2
Temperature (°C)	A	35	40	45	50	55
Pressure (bar)	B	80	120	160	200	240
Antisolvent addition rate (bar/min)	C	8	16	24	32	40
Polymer fraction (%)	D	0	10	20	30	40
Ethanol fraction (%)	E	0	25	50	75	100

Table 2. Central composite design matrix and experimental results

Run	Coded level of variables					Mean particle size (nm)		Solubility (mg/ml)	
	A	B	C	D	E	Experimental values	Predicted values	Experimental values	Predicted values
1	0	0	0	0	0	1,667	767	21.34	27.49
2	0	+2	0	0	0	495	481	12.06	8.73
3	0	0	−2	0	0	1,174	1,199	14.97	21.98
4	−1	1	1	−1	1	-	-	-	-
5	1	1	1	1	1	-	-	-	-
6	1	−1	1	1	−1	586	544	67.72	67.63
7	0	0	0	+2	0	329	195	38.18	39.56
8	−1	−1	1	−1	−1	585	659	82.77	86.09
9	0	0	0	0	0	685	767	26.54	27.49
10	0	0	+2	0	0	311	336	25.98	32.99
11	−1	−1	−1	−1	1	-	-	-	-
12	1	−1	−1	1	1	-	-	-	-
13	−1	−1	1	1	1	-	-	-	-
14	0	0	0	0	0	690	767	28.66	27.49
15	0	0	0	0	0	711	767	27.91	27.49
16	1	1	1	−1	−1	812	787	39.33	35.08
17	0	0	0	0	+2	-	-	-	-
18	−1	−1	−1	1	−1	715	690	20.01	23.34
19	+2	0	0	0	0	498	580	12.99	12.53
20	0	0	0	0	0	701	767	28.14	27.49
21	1	−1	1	−1	1	-	-	-	-
22	0	0	0	0	−2	316	710	8.76	48.25
23	−1	1	1	1	−1	600	593	11.58	12.59
24	1	1	−1	−1	1	-	-	-	-
25	−1	1	−1	−1	−1	975	933	58.32	59.33
26	0	0	0	0	0	966	767	26.37	27.49
27	−2	0	0	0	0	872	954	51.57	42.44
28	−1	1	−1	1	1	-	-	-	-
29	1	−1	−1	−1	−1	891	884	11.99	11.90
30	0	0	0	−2	0	1,474	1,340	14.03	15.41
31	1	1	−1	1	−1	744	818	11.18	6.93
32	0	−2	0	0	0	1,066	1,053	56.05	46.24

higher volume fraction of ethanol (more than 50%) produced inadequate precipitated particles to accumulate due to elimination through the mixture consisting of organic solvents and $scCO_2$. The experimental values of average particle size and solubility were in the range of 311-2,716 nm and of 8.76-82.77 mg/ml, respectively.

Among the linear and 2Fl models, the reduced 2Fl model is used to analyze two responses with the highest values of R^2 and significant p-value. Therefore, the experimental values are regressed using the selected models. The regression equations based on coded factors for the particle size (Y_1) and solubility (Y_2) responses are as follows:

$$Y_1=+767.11-93.38\,A-142.87\,B-215.75\,C-286.26\,D+28.63\,E-113.15\,AE-187.16\,BE-123.04\,CE-209.15\,DE \quad (2)$$

$$Y_2=+27.49-7.48\,A-9.38\,B+2.75\,C+6.04\,D-10.38\,E+8.48\,AC+17.13\,AD-9.73\,CE+16.27\,DE \quad (3)$$

The significance of coefficients and interaction between the independent model variables with p-value and F-value was evaluated. F-value and p-value of the models are reported as 13.55 and <0.0001 for particle size (Y_1), 27.72 and <0.0001 for solubility (Y_2), respectively, which indicates the model significance for both responses. The adequate precision for particle size and solubility is 15.4835 and 20.4660, respectively, which is greater than 4 and shows that the modeling is reliable. The R^2 value is 0.9172 and 0.9541 for Eqs. (2) and (3), respectively, implying that the correlations were optimal for a good fitting between the actual and predicted data (as shown in Fig. 2). The model's analysis of variance (ANOVA) is shown in Table 3 which examines the effect of coefficients on the particle size response. According to the ANOVA, the linear terms A, B, C, and D as well as interaction terms BE, CE, and DE were considered as significant terms of the model. Among these, the polymer fraction with the minimum p-value was the most signifi-

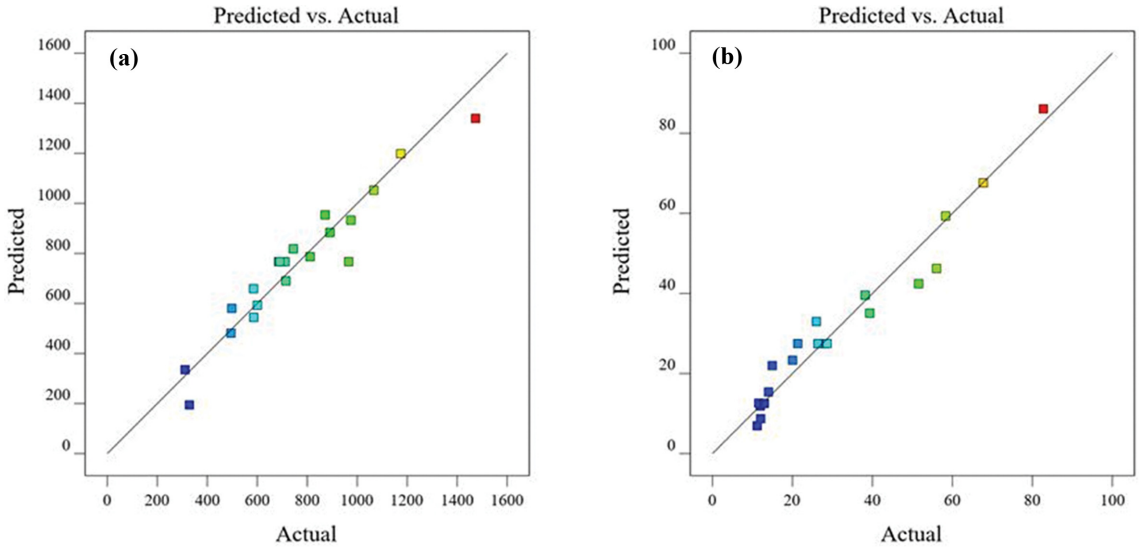

Fig. 2. The actual versus the predicted response values for (a) particle size, (b) solubility.

Table 3. Analysis of variance (ANOVA) of the RSM model for the particle size response. P<0.05 is significant

Source	Sum of squares	Degree of freedom	Mean square	F-value	p-Value
Model	1.400 E+06	9	1.556 E+05	13.55	<0.0001
A	69,766.07	1	69,766.07	6.07	0.0314
B	1.633 E+05	1	1.633E+05	14.22	0.0031
C	3.724 E+05	1	3.724E+05	32.42	0.0001
D	6.556 E+05	1	6.556E+05	57.08	<0.0001
E	4,059.98	1	4,059.98	0.3535	0.5642
AE	51,215.08	1	51,215.08	4.46	0.0584
BE	1.401 E+05	1	1.401E+05	12.20	0.0050
CE	60,554.14	1	60,554.14	5.27	0.0423
DE	1.750 E+05	1	1.750E+05	15.24	0.0025
Residual	1.263 E+05	11	11,485.13		
Lack of fit	68,060.97	7	9,723.00	0.6674	0.7000
Pure error	58,275.50	4	14,568.88		
Cor total	1.527 E+06	20			

Table 4. Analysis of variance (ANOVA) of the RSM model for the solubility response. P<0.05 is significant

Source	Sum of squares	Degree of freedom	Mean square	F-value	p-Value
Model	8,212.38	9	912.49	27.72	<0.0001
A	894.25	1	894.25	27.17	0.0002
B	1,407.25	1	1,407.25	42.76	<0.0001
C	60.65	1	60.65	1.84	0.1996
D	291.51	1	291.51	8.86	0.0116
E	548.24	1	548.24	16.66	0.0015
AC	575.77	1	575.77	17.49	0.0013
AD	2,348.68	1	2,348.68	71.36	<0.0001
CE	379.08	1	379.08	11.52	0.0053
DE	1,059.27	1	1,059.27	32.18	0.0001
Residual	394.95	12	32.91		
Lack of fit	358.96	7	51.28	7.12	0.0230
Pure error	35.99	5	7.20		
Cor total	8,607.33	21			

cant variable. The results show that ethanol fraction with the p-value of 0.5642 had no impact on the particle size, but its interaction with other variables was not negligible. The ANOVA for the solubility response is also presented in Table 4. These values show that factors A, B, D, and E as well as interaction terms AC, AD, CE, and DE are significant. Note that the pressure parameter (B) and interaction between temperature and polymer fraction (AD) had the greatest effect on the particle solubility.

2. Effect of Operating Conditions on PZA-PVP Particle Size

Three-dimensional (3D) response surface plots were formed to investigate the interaction effect of all five factors on the particle size (Fig. 3). The graphical visualization provides relationships between the experimental levels of each factor, the response, and the type of interaction effect between the variables, which is essential to find the optimum conditions of the GAS process. Fig. 3(a) shows the 3D plot of the interaction between temperature and ethanol fraction (AE) on the particle size at constant pressure (160 bar), antisolvent addition rate (24 bar/min), and polymer fraction (20%). Temperature and ethanol fraction can significantly affect $scCO_2$ solubility in the solvent mixture, supersaturation level, and hence particle precipitation. Minimum particle size was produced when the temperature was at the maximum level (50 °C) and ethanol fraction was moderate (50%). This could be explained as follows: reduction in solute solubility due to the supercritical fluid miscibility in organic solvent mixtures results in volumetric expansion of the liquid phase and accumulation of supersaturation, which induces particle precipitation in GAS processes [16,17]. Indeed, temperature augmentation causes reduced solubility of $scCO_2$ in pure solvents and solvent mixtures but increased solubility of solute in the solvent [32]. This operating condition may result in a challenge of solvent extraction and mass transfer, which leads to a reduction in nucleation rate and nuclei generation. Accordingly, agglomerates of discrete particles and growth rate become dominant and, consequently, increase the particle size. On the other hand, temperature rise causes reduction in viscosity and accretion of chain mobility in the polymer matrix, demonstrating enhanced mass transfer and particle size reduction. Besides, increasing ethanol content in the solvent mixture reduces solubility of the organic solvent in $scCO_2$, which in turn postpones nucleation and leads to particle growth [32]. Thus, there is an optimal point for achieving the desired results.

When the temperature was at a low level and ethanol content was slightly higher than moderate, particle size of the precipitated PZA-PVP was affected negatively.

The simultaneous effect of pressure and ethanol fraction (BE)

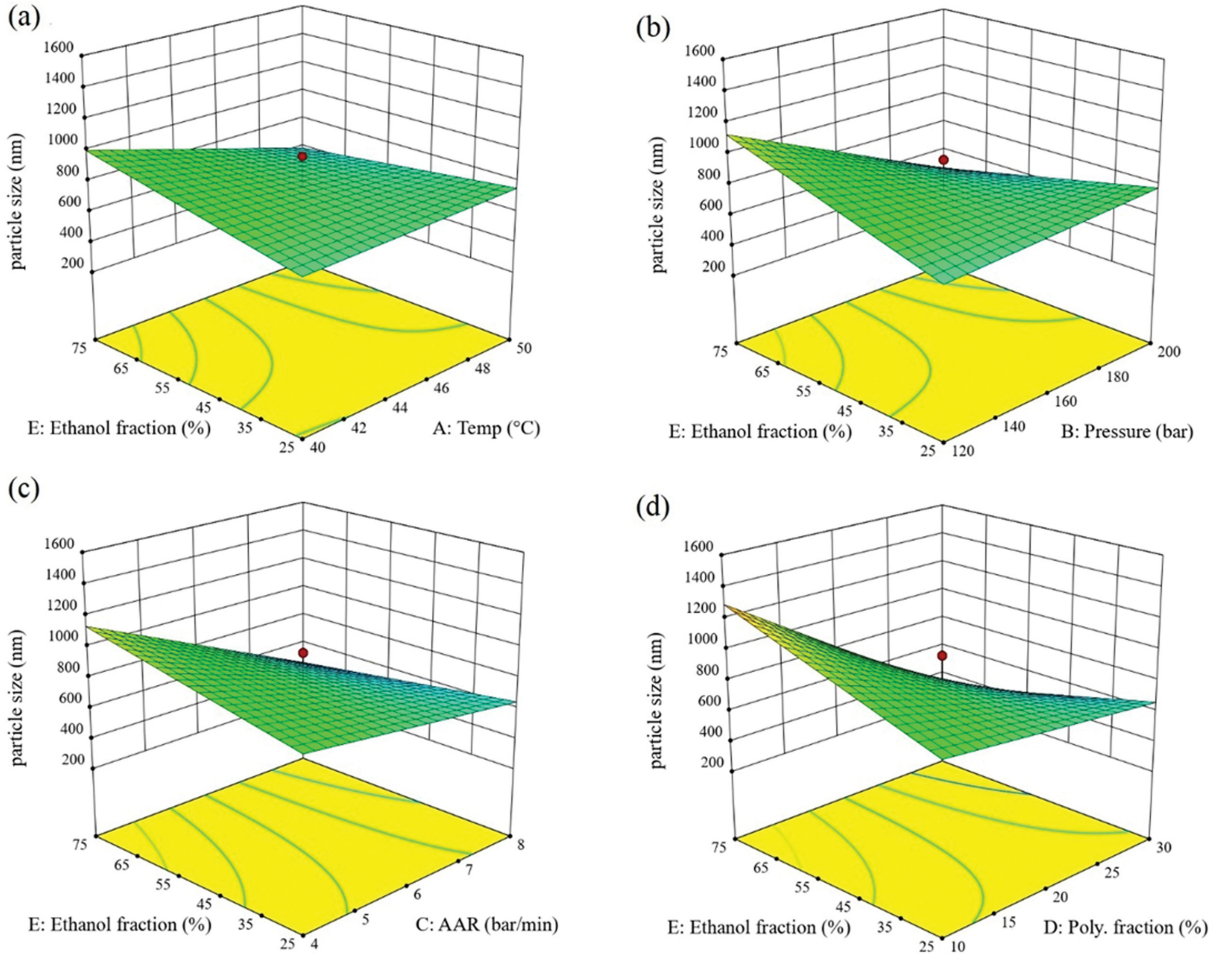

Fig. 3. The 3D surface plot indicating the interaction between (a) temperature and ethanol fraction, (b) pressure and ethanol fraction, (c) antisolvent addition rate (AAR) and ethanol fraction, (d) polymer fraction and ethanol fraction.

on the size of coprecipitated particles is also important (Fig. 3(b)). As it was evident, minimum particle size was achieved at higher pressures, while the ethanol fraction was moderate (50%). Conversely, the highest particle size was achieved when the pressure was at the minimum value and the ethanol fraction was at the maximum level. Evidently, increasing pressure significantly impacted CO_2 density and organic solvent diffusivity, which are the properties controlling the particle size. As the pressure increases, the density and the viscosity of CO_2 rise considerably and the diffusivity of the organic solvent decreases. Thus, mass transfer between droplets and their surroundings is prevented, which leads to increased droplet life, low supersaturation, low nucleation, and larger crystal size. On the other hand, atomization occurs at high pressures and CO_2 velocity increases; as a result, the jet break-up and turbulence after mixing solution increase, which reduces the droplet surface tension. This increases the solvent evaporation rate compared to CO_2 diffusion through the solvent followed by smaller particles. Therefore, the effect of pressure on particle size could be due to the interaction impact of mass transfer and atomization.

Fig. 3(c) demonstrates the effect of antisolvent addition rate and ethanol fraction (CE) on the size of coprecipitated powders while other independent variables were kept constant. As can be seen in Table 2 for runs 10, 14, and 3, when the antisolvent addition rate increased from 8 to 40 bar/min, the particle size increased from 311 to 1,174 nm at process pressure of 160 bar, polymer fraction of 20% and process temperature of 45 °C. Increasing the flow rate of CO_2 led to increasing kinetic energy between CO_2 and organic solvent followed by mass transfer improvement and increased supersaturation. However, some local supersaturation occurred by sudden entrance of $scCO_2$ to the precipitation chamber, which caused nucleation in particular places. Therefore, coprecipitated particles agglomerated, growth mechanism prevailed over nucleation, and larger particles were obtained.

The polymer fraction was varied to explore its effect on the mean particle size. As shown in Table 3, the polymer fraction was considered as the greatest factor, with the highest F-value of 57.08 (p-value<0.0001). Besides, the interaction of polymer fraction and ethanol fraction (DE) (Fig. 3(d)) significantly impacted the size of the produced particles (p-value of 0.0025). The smallest particles were achieved at the maximum polymer fraction and ethanol content in the organic solvent mixture. The experimental results show that higher concentration of polymer (more than 40% in polymer/drug mixture) negatively affected PZA-PVP particle size. As aforementioned, with increasing the polymer content, solution viscosity increased, which led to more agglomeration and making a sticky surface [28].

According to Fig. 3(d), the increased particle size can be seen in small amounts of polymer, which is due to the point that PVP polymer could control the particle growth. The effect of polymer content on particle size emerges in slightly high ethanol content (above 50%); since a high ethanol content was not efficient for the studied system, it was necessary to find an optimal point for the polymer content as well as the ethanol content in the organic solvent.

3. Effect of Operating Conditions on PZA-PVP Solubility

For the PZA-PVP solubility, the interaction of temperature and polymer fraction (AD) followed by pressure (B) were found to have substantial effect on the solubility of precipitated particles, with F-values of 71.36 and 42.76, respectively. However, the least important factor seemed to be the antisolvent addition rate, which represents the lowest F-value of 1.84 (Table 4). Since the interaction of temperature and polymer fraction positively affected solubility, a 3D graph and a contour plot for these two factors were generated (Fig. 4). It is evident that the maximum solubility was achieved when both parameters were at the maximum level. This was due to the point that, at higher concentrations of PVP, the solubility of PZA particles containing PVP improved significantly because of the solubilizing effect of PVP as a hydrophilic stabilizer [33-35]. As mentioned, the increment in temperature was associated with the decline in particle size. Therefore, the particle size reduction at high temperatures further intensified the effect of hydrophilic stabilizers for increasing solubility.

4. Process Optimization and Validation of Results

The main purpose of this work was to determine the optimal operating conditions relating to the size distribution and the solu-

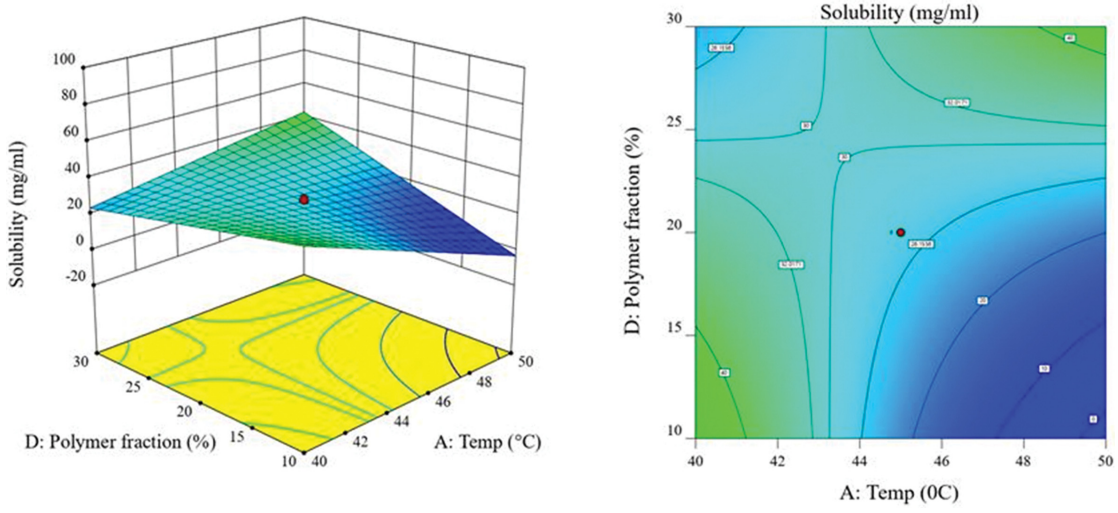

Fig. 4. The 3D surface and the contour plots indicating the interaction between temperature and polymer fraction for the solubility response.

Table 5. Optimal condition and model validation

Temperature (°C)	Pressure (bar)	Antisolvent addition rate (bar/min)	Polymer fraction (%)	Ethanol fraction (%)	Particle size (nm)		Solubility (mg/ml)	
					Predicted	Experimental	Predicted	Experimental
50	120	16	30	50	312	326	63.73	76.29

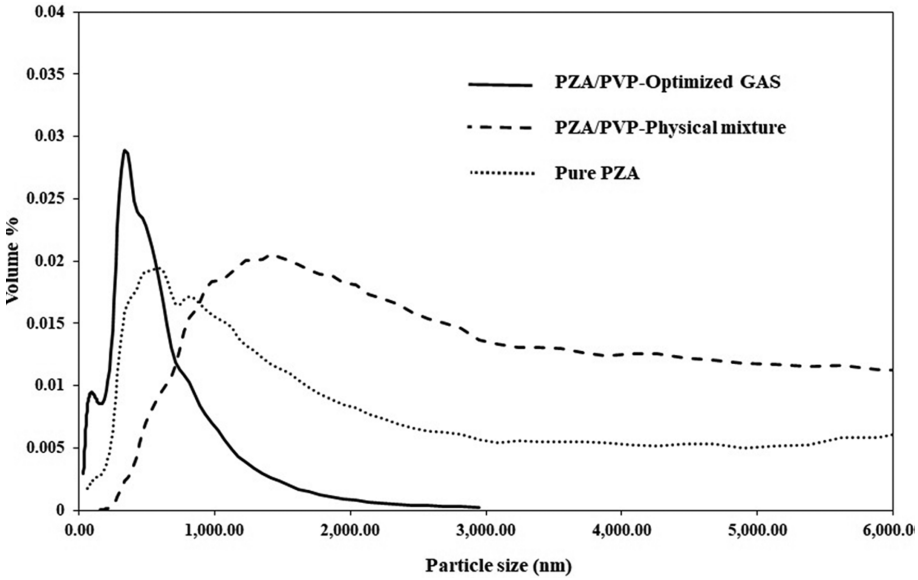

Fig. 5. Volumetric cumulative pure PZA, PZA-PVP particles obtained by physical mixture, and by optimized GAS.

bility of PZA-PVP particles produced by the GAS process. The desirability function could be a significant approach for multi-response optimization. Therefore, a series of experiments were considered with the maximum desirability to validate the model using the Design-Expert software version 12.0.3. The predicted and experimental data of mean particle size and solubility, under the estimated optimal conditions, are presented in Table 5. The optimized coprecipitated particles were obtained at 50 °C, 120 bar, antisolvent addition rate of 16 bar/min, ethanol fraction of 50%, and polymer fraction of 30%. In this condition, the predicted mean particle size was 312 nm and the predicted solubility was 63.73 mg/ml, which was close to the experimental values (326 nm and 76.29 for particle size and solubility, respectively). The validation results demonstrated that utilizing the RSM could be an effective tool for reaching particles with smaller size and higher solubility in GAS systems.

5. Characterization of Precipitated Particles under Optimum Conditions

The optimized PZA-PVP particles prepared by the GAS process were identified through DLS, XRD, and FTIR analyses, and were compared with the results from physical mixture and with pure PZA.

Fig. 5 shows the particle size distribution of pure PZA, submicron particles obtained in the optimal condition, and physical mixture. It was observed that optimized PZA-PVP particles using the GAS process presented narrower size distribution with a smaller particle mean size, in contrast to the other two cases. The prominent advantage of GAS processes, such as the considerable solvating power of $scCO_2$ in organic solvents, could pave the way for achieving higher supersaturation, followed by fast nucleation rates. Therefore, GAS process is a good candidate for incorporating active compounds into polymeric carriers to obtain particles with smaller size and narrower size distribution than using other methods.

XRD is a useful analytical technique for evaluating the crystalline structure of compounds. XRD patterns for pure PZA, pure PVP, physical mixture combination PZA and PVP, and optimized PZA-PVP precipitated by GAS process are illustrated in Fig. 6. It can be seen that pure PZA show sharp peaks at 2θ values of 13.77°, 15.35°, 17.65°, 23.71°, 26.47°, 35.87°, and 39.87°, which represent the crystalline nature of the drug [36]. Moreover, the amorphous state of PVP was identified through its pattern. The diffractogram of the physical mixture indicates a combination of diffraction patterns of the pure samples, but with less intensity, which is attributed to the amorphous nature of PVP. The PZA-PVP particles prepared by the GAS process in the optimal condition show that the intensity of characteristic peaks as at 15.35°, 17.65°, 35.87°, and 39.87° 2θ values seemed slighter. In fact, the GAS process led to forming smaller particles because of fast nucleation during the precipitation [26,37]. Moreover, the presence of a polymeric carrier helps the particle formation via converting a crystalline structure into an amorphous one.

FT-IR spectroscopy was employed to investigate possible interactions between PZA and PVP at the molecular level during coprecipitation. The FT-IR spectra of pure PZA, pure PVP, physical mixture, and coprecipitated particles prepared by the GAS process in optimal conditions are presented in Fig. 7. The characteristic peaks for pure PZA indicate the stretching vibration at 3,414 cm^{-1}, 3,290

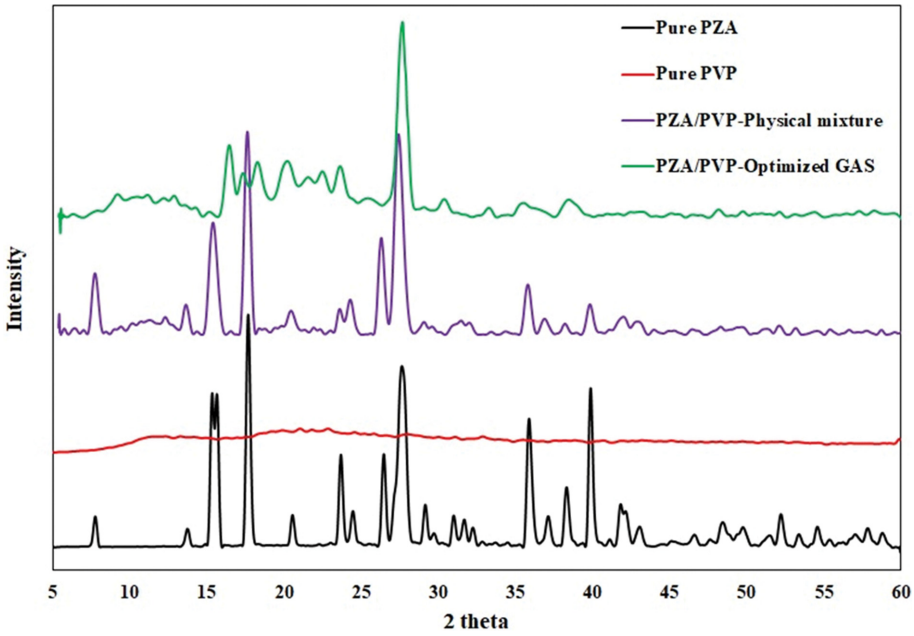

Fig. 6. XRD patterns of pure materials and PZA-PVP particles obtained by physical mixture, and by optimized GAS.

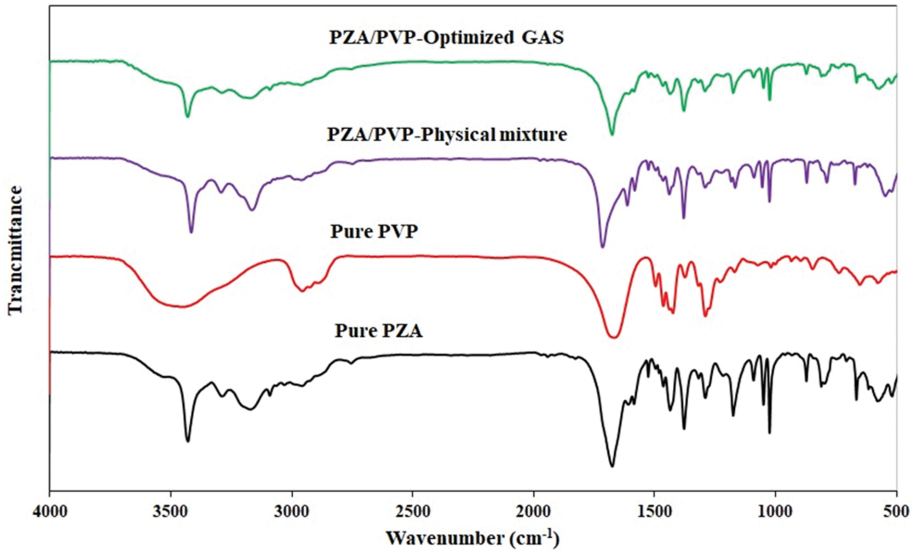

Fig. 7. FTIR spectra for pure materials and PZA-PVP particles obtained by physical mixture, and by optimized GAS.

cm^{-1}, and 3,164 cm^{-1} for N-H, and at 1,714 cm^{-1} for C=O. These results were previously diagnosed by Cherukuvada et al. [36]. The FT-IR spectra recorded from amorphous PVP exhibit important peaks at 3,450 cm^{-1} and 1,666 cm^{-1}. The broad peak at 3,450 cm^{-1} is attributed to the presence of water caused by the hygroscopic nature of PVP and those at 1,666 cm^{-1} correspond to the stretching vibration of C=O (carbonyl group). The FT-IR spectra of the physical mixture are in conformity with the pure samples, representing lack of molecular interaction between two substances during the simple mixing. The corresponding IR spectra of PZA-PVP particles obtained through the optimized GAS process have a different pattern from the pure drug and polymer. Accordingly, the peak at 1,674 cm^{-1} (attributed to the C=O bond) underwent a considerable reduction compared to the individual components. It was interpreted as the advent of intermolecular interaction between PZA and PVP. Besides, there is a broad spectrum at 3,428 cm^{-1} and a variation in the position of the N-H group for PZA, which exhibits the formation of an amorphous structure for the PZA-PVP particles obtained by the GAS process. Finally, the presence of a new peak at 2,958 cm^{-1} indicates the appearance of a hydrogen bond in this sample.

From the FESEM images Fig. 8(a), (b), it was found that precipitated particles prepared by the optimized GAS process reveal an amorphous state in which a substantial portion of drug is intertwined in the polymer matrix. Obviously, supercritical precipitation process causes variation of the morphology from semi-cylindrical

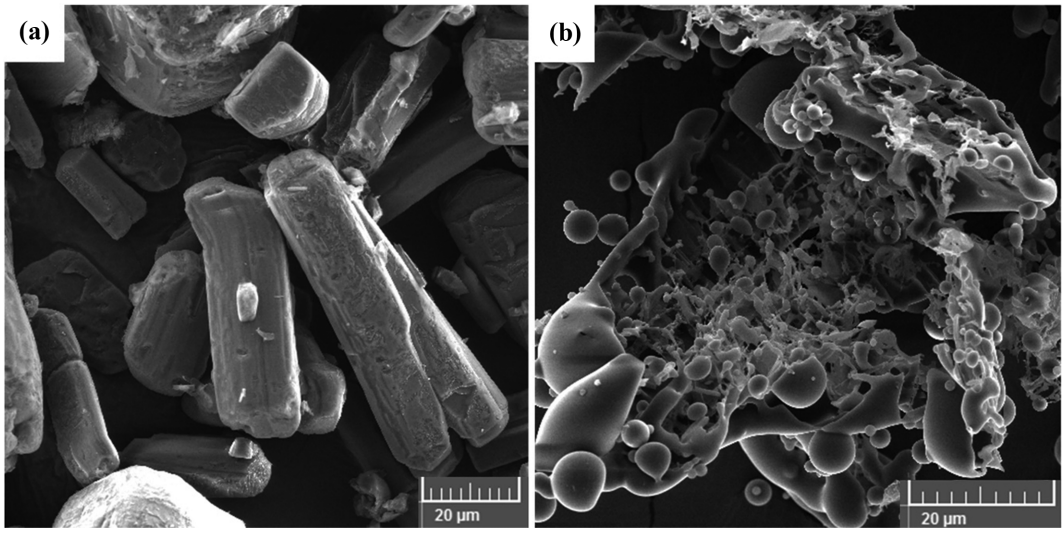

Fig. 8. FESEM images for (a) pure PZA, (b) optimized PZA-PVP particles.

(Fig. 8(a)) to almost porous structure (Fig. 8(b)). It can be due to the interaction of organic solvents dissolved in the $scCO_2$, and application of a suitable polymeric carrier which had a great effect on preventing crystallization.

CONCLUSION

Central Composite Design was applied to optimize GAS process parameters with the aim of reducing the particle size and increasing the solubility of PZA-PVP particles in the GAS process. Statistical analysis demonstrated that polymer fraction was a very effective parameter on preparation of smaller particles, while pressure and interaction between temperature and polymer fraction were the most significant factors for enhancing the solubility. The coprecipitated particles by the GAS process in the optimal condition showed a noteworthy narrower size distribution than the pure PZA and physical mixture. Furthermore, there was a 5.4-fold increase in solubility as compared to pure drug. The optimal coprecipitated particles were obtained at 50 °C temperature, 120 bar pressure, 16 bar/min antisolvent addition rate, 30% polymer fraction, and 50% ethanol fraction. The results subsequently showed that the optimized GAS process was a successful method for preparing PZA-PVP particles.

REFERENCES

1. A. Silva, B. Vieira, F. Carmo, L. Amaral, L. Silva, C. Escudini, M. Lopes, V. Sousa, H. Castro, F. Veiga, C. Rodrigues, A. Ribeiro and L. Cabral, *British J. Pharm. Res.*, **4**, 1781 (2014).
2. D. Maher, P. Chaulet, S. Spinaci and A. Harries, *Treatment of tuberculosis: guidelines for national programmes*, Second edition, 2 ed., World Health Organization, Geneva (1997).
3. R. Varma, T. S. Kumar, B. Prasanthi and J. V. Ratna, *Indian J. Pharm. Sci.*, **77**, 258 (2015).
4. G. Baaklini, V. Dupray and G. Coquerel, *Int. J. Pharm.*, **479**, 163 (2015).
5. U. S. Kestur and L. S. Taylor, *CrystEngComm*, **12**, 2390 (2010).
6. B. C. Hancock and M. Parks, *Pharm. Res.*, **17**, 397 (2000).
7. V. Prosapio, I. De Marco and E. Reverchon, *Chem. Eng. J.*, **292**, 264 (2016).
8. L. Padrela, J. Zeglinski and K. M. Ryan, *Cryst. Growth Des.*, **17**, 4544 (2017).
9. V. Prosapio, I. De Marco and E. Reverchon, *J. Supercrit. Fluids*, **138**, 247 (2018).
10. K. Moribe, Y. Tozuka and K. Yamamoto, *Adv. Drug Deliv. Rev.*, **60**, 328 (2008).
11. I. Pasquali, R. Bettini and F. Giordano, *Adv. Drug Deliv. Rev.*, **60**, 399 (2008).
12. F. Dehghani and N. R. Foster, *Curr. Opin. Solid State Mater. Sci.*, **7**, 363 (2003).
13. M. Amani, N. Saadati Ardestani and N. Y. Majd, *J. CO_2 Utilization*, **46**, 101465 (2021).
14. I. Garay, A. Pocheville and L. Madariaga, *Powder Technol.*, **197**, 211 (2010).
15. S. Varona, J. Fernández, M. Rossmann and A. Braeuer, *J. Chem. Eng. Data*, **58**, 1054 (2013).
16. A. Montes, M. D. Gordillo, C. Pereyra and E. J. Martínez de la Ossa, *J. Supercrit. Fluids*, **60**, 75 (2011).
17. I. De Marco, M. Rossmann, V. Prosapio, E. Reverchon and A. Braeuer, *Chem. Eng. J.*, **273**, 344 (2015).
18. N. Foster, R. Mammucari, F. Dehghani, A. Barrett, K. Bezanehtak, E. Coen, G. Combes, L. Meure, A. Ng, H. L. Regtop and A. Tandya, *Ind. Eng. Chem. Res.*, **42**, 6476 (2003).
19. A. Gokhale, B. Khusid, R. N. Dave and R. Pfeffer, *J. Supercrit. Fluids*, **43**, 341 (2007).
20. P. Franco, E. Reverchon and I. De Marco, *Powder Technol.*, **340**, 1 (2018).
21. A. Homayouni, F. Sadeghi, J. Varshosaz, H. A. Garekani and A. Nokhodchi, *Eur. J. Pharm. Biopharm.*, **88**, 261 (2014).
22. G. Ozkan, P. Franco, E. Capanoglu and I. De Marco, *Chem. Eng. Process. - Process Intensification*, **146**, 107689 (2019).
23. İ. N. Uzun, O. Sipahigil and S. Dinçer, *J. Supercrit. Fluids*, **55**, 1059

(2011).
24. F. Fusaro, M. Mazzotti and G. Muhrer, *Cryst. Growth Des.*, **4**, 881 (2004).
25. N. Esfandiari and S. M. Ghoreishi, *J. Supercrit. Fluids*, **84**, 205 (2013).
26. C. A. Ober, S. E. Montgomery and R. B. Gupta, *Powder Technol.*, **236**, 122 (2013).
27. D. Jafari, I. Yarnezhad, S. M. Nowee and S. H. N. Baghban, *Ind. Eng. Chem. Res.*, **54**, 3685 (2015).
28. A. Shirafkan, S. M. Nowee and H. Kamali, *J. Supercrit. Fluids*, **178**, 105386 (2021).
29. J. B. Ngilirabanga, M. Aucamp, P. Pires Rosa and H. Samsodien, *Front. Chem.*, **8**, 1051 (2020).
30. D. Medarević, J. Djuriš, S. Ibrić, M. Mitrić and K. Kachrimanis, *Int. J. Pharm.*, **540**, 150 (2018).
31. Z. Zhang, Q. Li, B. Guo, S. Zhang, S. Zhang and D. Hu, *Sci. Rep.*, **10**, 11187 (2020).
32. R. Campardelli, E. Reverchon and I. De Marco, *J. Supercrit. Fluids*, **143**, 321 (2019).
33. V. Prosapio, E. Reverchon and I. De Marco, *J. CO_2 Utilization*, **19**, 230 (2017).
34. K. Chhouk, Wahyudiono, H. Kanda, S.-I. Kawasaki and M. Goto, *Front. Chem. Sci. Eng.*, **12**, 184 (2018).
35. W. J. Gun and A. F. Routh, *Langmuir*, **29**, 12541 (2013).
36. S. Cherukuvada, R. Thakuria and A. Nangia, *Cryst. Growth Des.*, **10**, 3931 (2010).
37. A. M. Barrett, F. Dehghani and N. R. Foster, *Pharm. Res.*, **25**, 1274 (2008).